

Molecular Modeling of the Human Hemoglobin-Haptoglobin Complex Sheds Light on the Protective Mechanisms of Haptoglobin

Chanin Nantasenamat^{1,2}, Virapong Prachayasittikul², Leif Bulow^{3*}

1 Center of Data Mining and Biomedical Informatics, Faculty of Medical Technology, Mahidol University, Bangkok, Thailand, **2** Department of Clinical Microbiology and Applied Technology, Faculty of Medical Technology, Mahidol University, Bangkok, Thailand, **3** Pure and Applied Biochemistry, Department of Chemistry, Lund University, Lund, Sweden

Abstract

Hemoglobin (Hb) plays a critical role in human physiological function by transporting O₂. Hb is safe and inert within the confinement of the red blood cell but becomes reactive and toxic upon hemolysis. Haptoglobin (Hp) is an acute-phase serum protein that scavenges Hb and the resulting Hb-Hp complex is subjected to CD163-mediated endocytosis by macrophages. The interaction between Hb and Hp is extraordinarily strong and largely irreversible. As the structural details of the human Hb-Hp complex are not yet available, this study reports for the first time on insights of the binding modalities and molecular details of the human Hb-Hp interaction by means of protein-protein docking. Furthermore, residues that are pertinent for complex formation were identified by computational alanine scanning mutagenesis. Results revealed that the surface of the binding interface of Hb-Hp is not flat and protrudes into each binding partner. It was also observed that the secondary structures at the Hb-Hp interface are oriented as coils and α -helices. When dissecting the interface in more detail, it is obvious that several tyrosine residues of Hb, particularly β 145Tyr, α 42Tyr and α 140Tyr, are buried in the complex and protected from further oxidative reactions. Such finding opens up new avenues for the design of Hp mimics which may be used as alternative clinical Hb scavengers.

Citation: Nantasenamat C, Prachayasittikul V, Bulow L (2013) Molecular Modeling of the Human Hemoglobin-Haptoglobin Complex Sheds Light on the Protective Mechanisms of Haptoglobin. PLoS ONE 8(4): e62996. doi:10.1371/journal.pone.0062996

Editor: Franca Fraternali, King's College, London, United Kingdom

Received: July 23, 2012; **Accepted:** March 30, 2013; **Published:** April 26, 2013

Copyright: © 2013 Nantasenamat et al. This is an open-access article distributed under the terms of the Creative Commons Attribution License, which permits unrestricted use, distribution, and reproduction in any medium, provided the original author and source are credited.

Funding: The following research funding agencies are gratefully acknowledged for supporting the research performed: the Office of the Higher Education Commission, Mahidol University under the National Research Universities' Initiative, Swedish Research Foundation (VR) and Swedish Research Links. The funders had no role in study design, data collection and analysis, decision to publish, or preparation of the manuscript.

Competing Interests: The authors have declared that no competing interests exist.

* E-mail: Leif.Bulow@tbiokem.lth.se

Introduction

Hemoglobin (Hb) is a ubiquitous protein found in all kingdoms of life, i.e. in archaea, bacteria, fungi, protists, plants and animals [1]. It can inherently bind gaseous diatomic ligands such as O₂, CO and NO via its heme prosthetic group, which is bound to the protein via the axial histidine ligands. Human HbA is a tetrameric structure comprising of two $\alpha\beta$ dimers. The globin-fold of each monomeric chain is comprised of eight helices with A, E and F helices stacking on top of B, G and H helices. Such structural topology is known as the 3-on-3 α -helical sandwich-fold while the 2-on-2 α -helical sandwich-fold, which is found in truncated Hb, places the B and E helices on top of the G and H helices. This globin-fold harbours the heme prosthetic group via coordination to the axially ligated histidine residues at the proximal and distal locations on the F and E helices, respectively.

Inside the erythrocyte, Hb is in a tetrameric form where it is present in the reduced and nontoxic state owing to a wide range of protective enzymatic systems [2–4]. However, upon intravascular hemolysis, caused e.g. by hemolytic anemias, autoimmune transfusion reactions, preeclampsia or intraventricular hemorrhage and subarachnoidal bleeding [3], it separates easily into agile dimeric forms that quickly can cause oxidative toxicity. Haptoglobin (Hp), which was first identified by Polonovski and

Jayle in 1938 [5], is an Hb scavenger that prevents many of the toxic effects caused by Hb. Hp is just like Hb, a tetrameric protein of four chains with molecular weights of 9 and 33 kDa, respectively, for each of the two α -chains and β -chains. This form of haptoglobin is called Hp 1-1, but the protein is also present in several different oligomeric structures which harbour a different α -chain [3]. Hp is an acute phase-plasma glycoprotein of the α_2 -globulin fraction found in plasma of humans and mammals [6]. Owing to its innate Hb binding property, Hp can effectively protect renal functions as well as provide other valuable physiological properties such as acting as an anti-inflammatory agent, antioxidant, angiogenic promoter, immune cell regulator and therapeutic agent of sickle cell disease [7]. This can be explained on the molecular level, since Hp counters the deleterious effects of toxic cell-free Hb by forming a very strong and specific Hb-Hp complex. This is today considered to be one of the strongest molecular interactions ($K_d = 10^{-14}$ M) known in nature [8]. The Hb-Hp conjugate is then rapidly bound to the macrophage membrane protein CD163 followed by its engulfment and degradation. The utilization of this specific Hp-Hb interaction with CD163 represents an important potential clinical tool for modulating the physiological status of macrophages, e.g. by controlling an inflammatory response.

The endeavors to get a better understanding on how Hb and Hp bind have resulted in a series of experimental investigations, which have slowly accumulated over the years. Such efforts have shed light on the Hb and Hp-binding sites on each protein. The Hb-binding site encompasses residues 121–135 [9] and 139–141 [10] of Hb α -chain and residues 11–25, 37 and 131–146 [11] of Hb β -chain. Likewise, the Hb-binding site comprises of residues 9–10, 128–131, 136–137 [12], 136, 218 [13], 137 [14] and 234–264 [15] of the Hp β -chain. Surprisingly, residues 1–70 on Hp α -chain [15] have also been suggested.

Preliminary information on the structural insights of Hb-Hp complex have also previously been provided by electron microscopic studies, which indicated that the Hb dimer interacts with Hp β -chain forming an angle of 127° relative to the axis of Hp [16]. In spite of this, the structural detail of this complex is not fully understood. Almost two decades later, Przybylska et al. [17] attempted to crystallize the Hb-Hp complex, however the crystals did not diffract well enough for data collection, which largely shortcut further investigations. Molecular modeling has frequently been instrumental for dissecting a range of biological phenomena [18–23] and is ever more important in contributing to better understanding of protein-protein interactions [24–27]. In this study, we have therefore examined the structural basis and binding modalities governing the interaction between Hb and Hp 1–1. This was achieved by first obtaining an ensemble of energetically stable conformers of Hb and Hp from the last 10 ns of molecular dynamics simulations. Such structures were subsequently docked using an extensive set of biochemical, structural and biophysical data as restraints to drive the docking calculations. Hot-spot residues of each binding partner were identified by means of computational alanine scanning mutagenesis. We were also specifically studying the structural details of the Hb tyrosine residues in the complex since these are known to be involved in toxic redox reactions [28].

Materials and Methods

Preparation of protein structures

The crystal structure of human Hb containing a single $\alpha\beta$ dimer was obtained from the Protein Data Bank (accession number 2DN1) [29] while the homology models of haptoglobin variant 1 was obtained from the Protein Model DataBase (accession number PM0075389) [30]. The N-terminal valine residues of α and β subunits of hemoglobin, which were not present in the structure, were modeled in using PyMol [31]. Coordinates of the heteroatoms, toluene and oxygen, were removed from the structure. The protonation state of histidines and other ionizable residues were assigned to the hemoglobin structure according to the structure of human hemoglobin determined at pH 6.7 via neutron crystallography [32,33]. For comparative purposes, the protonation states of ionizable residues in Hp were determined at pH 6.7 by the PDB2PQR web server [34] according to the PROPKA method [35]. Hydrogen atoms were then added to the structures using the *pdb2gmx* utility as provided by the GROMACS simulation package.

Molecular dynamics simulation

Molecular dynamics (MD) simulations were performed using the GROMOS 43A1 force field [36] with GROMACS version 4.0.5 [37]. A preliminary energy minimization of the protein structures was performed *in vacuo* in order to remove unfavorable van der Waals contacts. The minimization was performed for a maximum of 5,000 steps using the steepest descent algorithm. The convergence criterion of the energy minimization is reached when

the maximum force is less than $10 \text{ kJ mol}^{-1} \text{ nm}^{-1}$ or until no significant improvement can be attained between-steps.

The protein was placed at the center of a rhombic dodecahedral box solvated with single point charge (SPC) water molecules. The minimum distance between the protein and the wall of the simulation box was set to 1.5 nm. Periodic boundary conditions were applied in order to solve the issue of surface effects as well as to simulate bulk systems. Physiological ionic strength of 0.15 M NaCl was applied as counter-ions in order to equilibrate the system. Another round of energy minimization was performed on the solvated system using the procedures described above.

Two phases of equilibration were conducted under constant Number of particles, Volume and Temperature (NVT) followed by keeping the Number of particles, Pressure and Temperature (NPT) constant. The NVT ensemble was performed in two stages where in the first stage, the system was slowly heated over a time of 200 ps to bring the temperature to 200 K by randomly assigning initial velocities taken from Maxwell–Boltzmann distribution. Positional restraints were applied on the protein as to allow solvent molecules to relax around the structure. In the second stage, positional restraints were lifted and the system was coupled to a heat bath at 300 K using the Berendsen [38] thermostat and allowed to equilibrate for 200 ps. In an NPT ensemble, the Berendsen barostat was used for controlling the pressure to 1 atm with a compressibility of $4.5 \times 10^{-5} \text{ bar}^{-1}$. Time constants for controlling the temperature (τ_T) and pressure (τ_P) were set to 0.1 and 1 ps, respectively.

The production run was performed for 20 ns at a temperature and pressure of 300 K and 1 atm, respectively, according to the aforementioned settings and simulation. Snapshots were collected every 1 ns using an integration time step of 2 fs. For all MD simulations, the reaction field method [39] was used to treat long-range electrostatic interactions applying cutoff distances of 1.4 nm for both Coulomb and van der Waals interactions and a dielectric constant of 78 was applied for electrostatic interactions beyond 1.4 nm. The short-range neighbor list of 0.9 nm was used. Bond lengths were constrained using the Linear Constraint Solver (LINCS) algorithm [40].

Analysis of MD trajectories was performed using utilities within the GROMACS package.

Protein-protein docking calculation

The interaction of Hb and Hp was simulated by means of protein-protein docking calculation using HADDOCK server [41,42], which is an approach that incorporates biochemical and biophysical data to drive the docking process. HADDOCK achieves this by employing ambiguous interaction restraints that are known about the binding interface. Thus, residues that have previously been determined to be involved at the Hb-Hp binding interface were designated as active residues if they are also solvent exposed. This surface exposure was determined by GETAREA using criteria of greater than 40% solvent accessibility. Residues within a vicinity of 6.5 Å from active residues were designated as passive residues if they are also solvent exposed. Such lists of active and passive residues (as shown in Table 1) were used as ambiguous interaction restraints. Unambiguous restraints between the iron atom and nitrogen atoms of coordinating histidine residues were also defined. Finally, an ensemble of structures from the last 10 ns of MD simulation was cross-docked to give rise to a matrix of 10×10 different combinations. A positional RMSD cutoff of 7.5 Å was used for clustering docking solutions; it should be noted that only clusters with at least 5 structures were considered.

Table 1. Summary of interaction restraints used in protein-protein docking.

	Residues
<i>Ambiguous interaction restraints</i>	
Hb	
Active residues	α Lys127, α Ala130, α Thr134, α Lys139, α Arg141, β Thr12, β Ala13, β Gly16, β Lys17, β Asn19, β Glu22, β Trp37, β Ala135, β Asn139, β His143, β Lys144, β Tyr145, β His146
Passive residues	α Val1, α Ser3, α His89, α Arg92, α Ser138, β Lys8, β Ser9, β Pro36, β Arg40, β Ser72, β Thr87, β Glu90, β Lys95, β Leu96, β His97, β Glu101, β Arg104
Hp	
Active residues	β Lys9, β Phe129, β Lys130, β Phe131, β His134, β Asp144, β Asp146, β Arg150, β Thr156, β Val157, β Pro158, β Glu159, β Lys160, β Lys161, β Thr162, β Leu203, β Glu204, β Glu205, β Asp206, β Lys218, β Val222
Passive residues	α Asn36, α Lys76, α Asn77, β Leu6, β Ala8, β Asn23, β Thr61, β Glu99, β Lys109, β Val114, β Asn126, β Ala127, β His151, β Pro163, β Ser183
Hp $_{\beta}$ *	
Active residues	β Lys9, β Lys130, β Phe131, β Asp144, β Asp146, β Arg150, β Thr156, β Val157, β Glu159, β Lys160, β Lys161, β Thr162, β Leu203, β Glu204, β Glu205, β Asp206, β Val222, β Ala223
Passive residues	β His5, β Leu6, β Ala8, β Val64, β Glu99, β Val114, β Pro163, β Lys164, β Leu173, β Ser183, β Ser184, β Gln186, β Glu187
<i>Unambiguous interaction restraints</i>	
Hb	HemeFe-N $_{\alpha}$ His87
	HemeFe-N $_{\beta}$ His92

*Haptoglobin without α chain.

doi:10.1371/journal.pone.0062996.t001

Analysis of protein-protein interface

PISA [43] was used to analyze the Hb-Hp structures and binding interfaces from the top ten Hb-Hp docking models. The size of the protein-protein binding interface was calculated from the solvent accessible surface area (SASA) according to the following equation:

$$SASA_{\text{Interface}} = SASA_{\text{Hb}} + SASA_{\text{Hp}} - SASA_{\text{Hb-Hpcomplex}}$$

PROTORP [44] was then employed to assess the geometrical parameters of the protein complex. Gap volume index is a parameter that accounts for shape complementarity of the interface and is calculated according to the following equation:

$$\text{Gapindex(A)} = \frac{\text{Gapvolumebetweenmolecules(A}^3\text{)}}{\text{InterfaceSASA(A}^2\text{)}}$$

Hot spot calculation

Computational alanine scanning mutagenesis was performed to identify hot spots of protein-protein interaction using the graphical interface plugin [45] of FoldX [46] empirical force field for Yasara [47]. FoldX is an empirical force field that was formulated by analyzing 1,000 point mutations from 82 protein-protein complexes. The FoldX energy function accounts for several thermodynamic terms that are known to be important for protein stability, which includes van der Waals interactions, solvation effects, hydrogen bonds, water bridges, electrostatic and entropy effects for the backbone and the side-chain.

In this study, Hb-Hp interfacial residues were sequentially mutated to alanine and their energetic difference were calculated

as shown in the following equation:

$$\Delta\Delta G_{\text{binding}} = \Delta G_{\text{binding-mutant}} - \Delta G_{\text{binding-wildtype}}$$

where $\Delta\Delta G_{\text{binding}}$ represents the binding energy difference of mutant and wild-type, $\Delta G_{\text{binding-mutant}}$ represents the binding energy of mutant and $\Delta G_{\text{binding-wildtype}}$ represents the binding energy of wild-type.

The binding energy of Hb and Hp is calculated as the difference of the complex and its respective monomers as follows:

$$\Delta G_{\text{binding}} = \Delta G_{\text{complex}} - (\Delta G_{\text{Hb}} + \Delta G_{\text{Hp}})$$

where $\Delta G_{\text{binding}}$ is the binding energy for either the mutant or wild-type, $\Delta G_{\text{complex}}$ is the energy of Hb-Hp complex, ΔG_{Hb} is the energy of Hb and ΔG_{Hp} is the energy of Hp. Residues giving rise to $\Delta\Delta G_{\text{binding}} \geq 1.5$ kcal/mole were identified as potential hot spots.

Results and Discussion

Both human Hb and Hp 1-1 are tetramers comprised of two $\alpha\beta$ dimers where the former adopts a 3-on-3 α -helical globin fold and the latter takes the form of a linear dumbbell-shaped conformation [16]. The two $\alpha\beta$ -subunits of Hp form the aforementioned linear conformation as a result of the disulfide bond cross-linkage of the two α -chains of the $\alpha\beta$ -subunits. An electron microscopic study by Wejman et al. [16] provided early insights on the molecular topology of the Hb-Hp complex where one tetrameric $\alpha_2\beta_2$ molecule of Hp can interact with two $\alpha\beta$ dimer of the tetrameric $\alpha_2\beta_2$ Hb, particularly, the β -chain of Hp can interact with the $\alpha\beta$ dimer of Hb. This study aims to further elucidate the interaction of Hb-Hp complex at the molecular level through the use of molecular

dynamics and protein-protein docking methods, particularly focusing on how Hp can protect against toxic Hb radical formation.

Preparation of Hb and Hp structures

This study employs the crystal structure of a single $\alpha\beta$ dimer of Hb and the homology modeled structure of the $\alpha\beta$ dimer of Hp 1-1. The protein structures were then prepared for subsequent MD and docking simulations by removing heteroatoms as well as assigning appropriate protonation states for histidines and ionizable residues.

To discern the influence of the Hp α -chain on Hb-Hp interaction, a structural model of Hp was prepared in the absence of the α -chain and the resulting structure will be called Hp β -chain and abbreviated as Hp $_{\beta}$ from hereon. This structure was subjected to the same computational protocol as the other proteins.

Molecular dynamics of Hb and Hp/Hp $_{\beta}$

Molecular dynamics was employed to allow conformational relaxation of the structures before subjecting them to further protein-protein docking calculations. From Figure 1, it can be seen that all structures displayed an initial structural rearrangement that is followed by convergence to an RMSD plateau indicating minimal structural fluctuations during the latter part of the simulation. The overall structural fluctuation of Hb (Figure 1a) was observed to be less than that of Hp (Figure 1b) with an RMSD of 0.2 nm and 0.35 nm, respectively, which is to be expected as the protein structure of the former was obtained from X-ray crystallographic experiment (with a high resolution of 1.25 Å) while the latter was obtained from homology modeling. Furthermore, upon splitting the Hp structure into two separate domains, namely α - and β -chains (Figures 1c and 1d), it was observed that both chains displayed significantly different structural fluctuations with an RMSD of 0.9 and 0.2 nm, respectively, suggesting the former to be significantly more flexible than the latter chain. It should be noted that the large movement observed for the C-terminus of the α -chain and its apparently greater flexibility is perhaps not completely unexpected, due to the fact that the α -chain is truncated (13 residue missing) and to the lack of the disulfide bond between Cys15 of the α -chain and Cys15 of the partner α -chain that is missing in the model. It is also worthy to note that the two α -chains are in tight contact to each other. An ensemble of structures from the last 10 ns of MD simulation for Hb, Hp and Hp $_{\beta}$ were then used for further docking calculations (Figure 2).

Docking Hb to Hp/Hp $_{\beta}$

The biochemical, structural and biophysical data obtained from previous investigations that had assimilated over the years were used as ambiguous interaction restraints to drive the docking protocol using HADDOCK. This is comprised of 18, 21 and 18 active residues for Hb, Hp and Hp $_{\beta}$, respectively, while there are 17, 15 and 13 passive residues for Hb, Hp and Hp $_{\beta}$, respectively. A cut-off value of 7.5 Å was used for clustering solutions of the protein-protein complexes, which gave rise to a total of 281 and 259 structures in 17 and 16 clusters, respectively, for Hb-Hp and Hb-Hp $_{\beta}$. It should be noted that the largest cluster (and also the top ranking cluster) had 87 and 89 structures, respectively, for Hb-Hp and Hb-Hp $_{\beta}$ with a positional RMSD of 2.35 and 2.53 Å amongst the members, thus indicating moderately low structural variability within the clusters. Selection of the best representative cluster was made on the basis of the lowest HADDOCK score, which was 13.43 and 31.76 for Hb-Hp and Hb-Hp $_{\beta}$, respectively. It should be noted that the HADDOCK score represents a combination of energy terms that was calculated in relation to the

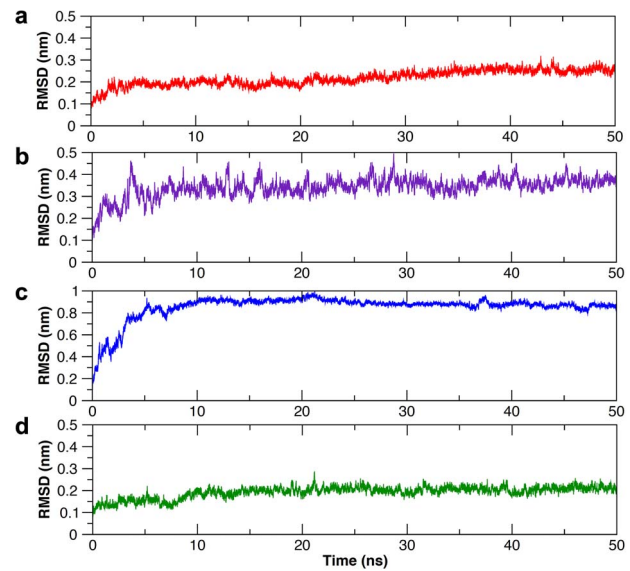


Figure 1. Structural fluctuation from MD simulation as described in terms of RMSD as a function of time for Hb (a), Hp (b), Hp $_{\alpha}$ (c) and Hp $_{\beta}$ (d).

doi:10.1371/journal.pone.0062996.g001

buried surface area value. The top ranked structure for Hb-Hp and Hb-Hp $_{\beta}$ from the best cluster is shown in Figures 3 and 4, respectively, from the side and top views. Residues at the binding interfaces of Hb-Hp and Hb-Hp $_{\beta}$ are shown in Figures 5 and 6, respectively.

Analysis of Hb-Hp and Hb-Hp $_{\beta}$ binding interface

Putative interface residues identified by PISA in the top ten models of Hb-Hp indicated an average of 33.8 ± 4.5 (ranging from 25 to 39) and 33.3 ± 4.9 (ranging from 26 to 40) residues of Hb and Hp, respectively, at the binding interface. It was observed that the interface area occupied $1146.4 \pm 181 \text{ \AA}^2$ (ranging from 835.1 to 1389.9) or roughly 6.1 and 6.9% of the SASA of Hb and Hp with SASA of 16708.6 ± 141.9 and $18848 \pm 145.4 \text{ \AA}^2$, respectively. Of all the putative interface residues identified by PISA, consensus residues found in seven of the top ten Hb-Hp models from the HADDOCK calculation are shown in Tables 2 and 3 for Hb-Hp and Hp $_{\beta}$ -Hp, respectively. The number of continuous interface residue segment for Hb-Hp was found to be 14 ± 0.9 (ranging from 12 to 15) as calculated from PROTORG. The gap volume index of Hb-Hp was $5.1 \pm 1 \text{ \AA}$, which is typical of non-obligate interaction (where each binding partner can exist individually as functional proteins whereas obligates cannot). Nooren and Thornton [42] noted that interfaces of transient complexes have small, planar and polar interface area as compared to those of homodimers. Planarity is a measure of the shape of the binding interface that is the flatness of an interface. The results show that the protein complex had a significantly less planar surface at the interface with a planarity value of $3.6 \pm 0.4 \text{ \AA}$ as compared to the average planarity of protein-protein interfaces of $3 \pm 0.5 \text{ \AA}$ [48]. This indicated that the protein interface is not flat and that there is protrusion into both binding partner. Results from PROTORG analysis pointed out that the secondary structures at the binding interface included coils and α -helices. Additionally, an estimate of the relative distribution of the polarity of surface exposed residue was carried out. Surface exposed residues were categorized into 3 classes: low polarity (Leu, Ile, Phe, Trp, Cys, Met, Val and Tyr), neutral polarity (Pro, Ala, Thr, Gly and Ser) and high polarity

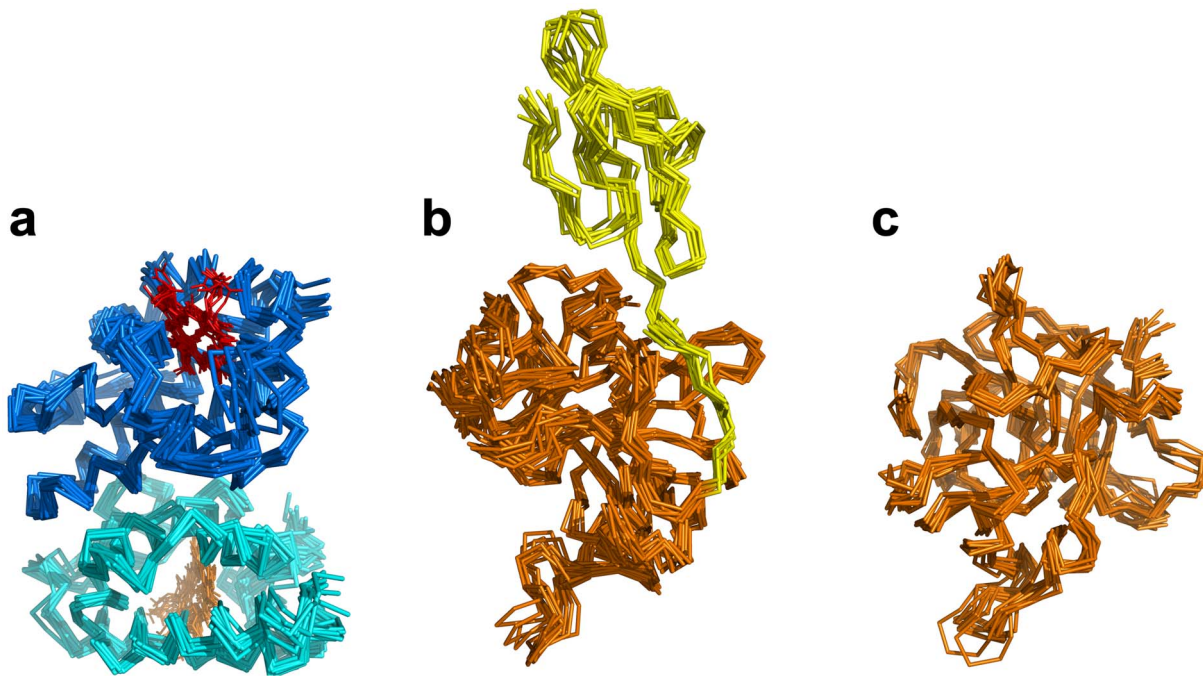


Figure 2. Ensemble of structures from the last 10 ns of MD simulation for Hb (a), Hp (b) and Hp β (c).
doi:10.1371/journal.pone.0062996.g002

(His, Asp, Glu, Asn, Gln, Arg and Lys). We found that surface exposed residues of Hb and Hp monomers before complexation had 36, 67 and 123 residues belonging to the low, neutral and high polarity classes, respectively, or approximately 15.9%, 29.6% and

54.4%, respectively, of the residues. After Hb-Hp complex formation the buried residues or those right at the binding interface are composed of 5, 10 and 10 residues, respectively, corresponding to 20%, 40% and 40%, respectively, of the

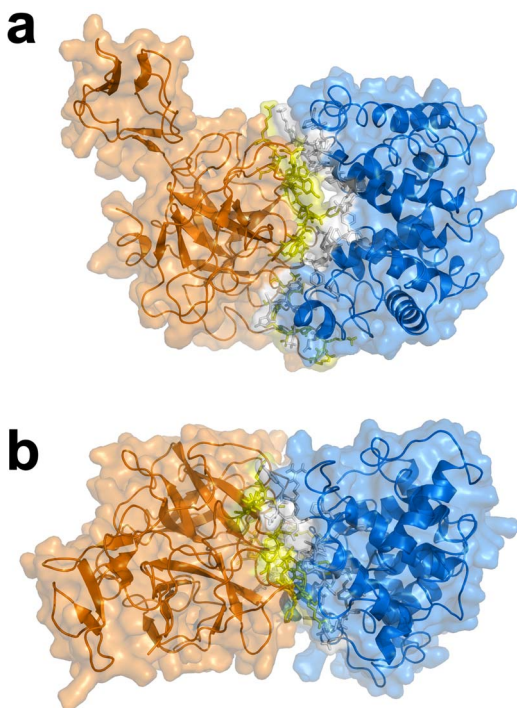


Figure 3. Top ranked structure of Hb-Hp from the best cluster of docking simulation is shown from the side (a) and top (b) view.
doi:10.1371/journal.pone.0062996.g003

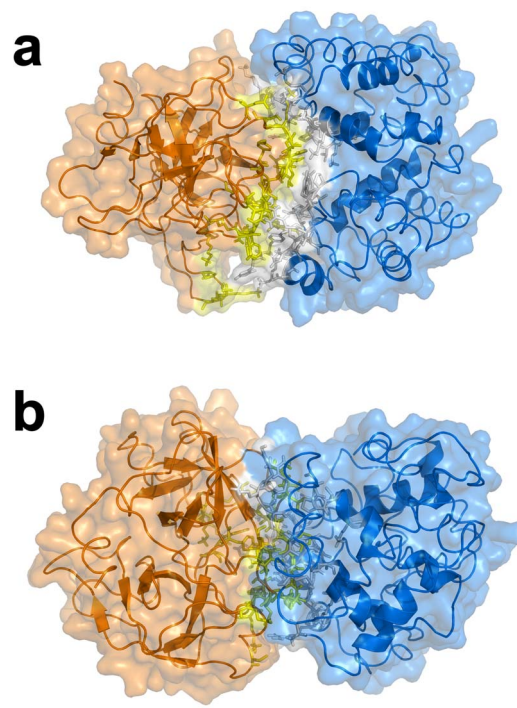


Figure 4. Top ranked structure of Hb-Hp β from the best cluster of docking simulation is shown from the side (a) and top (b) view.
doi:10.1371/journal.pone.0062996.g004

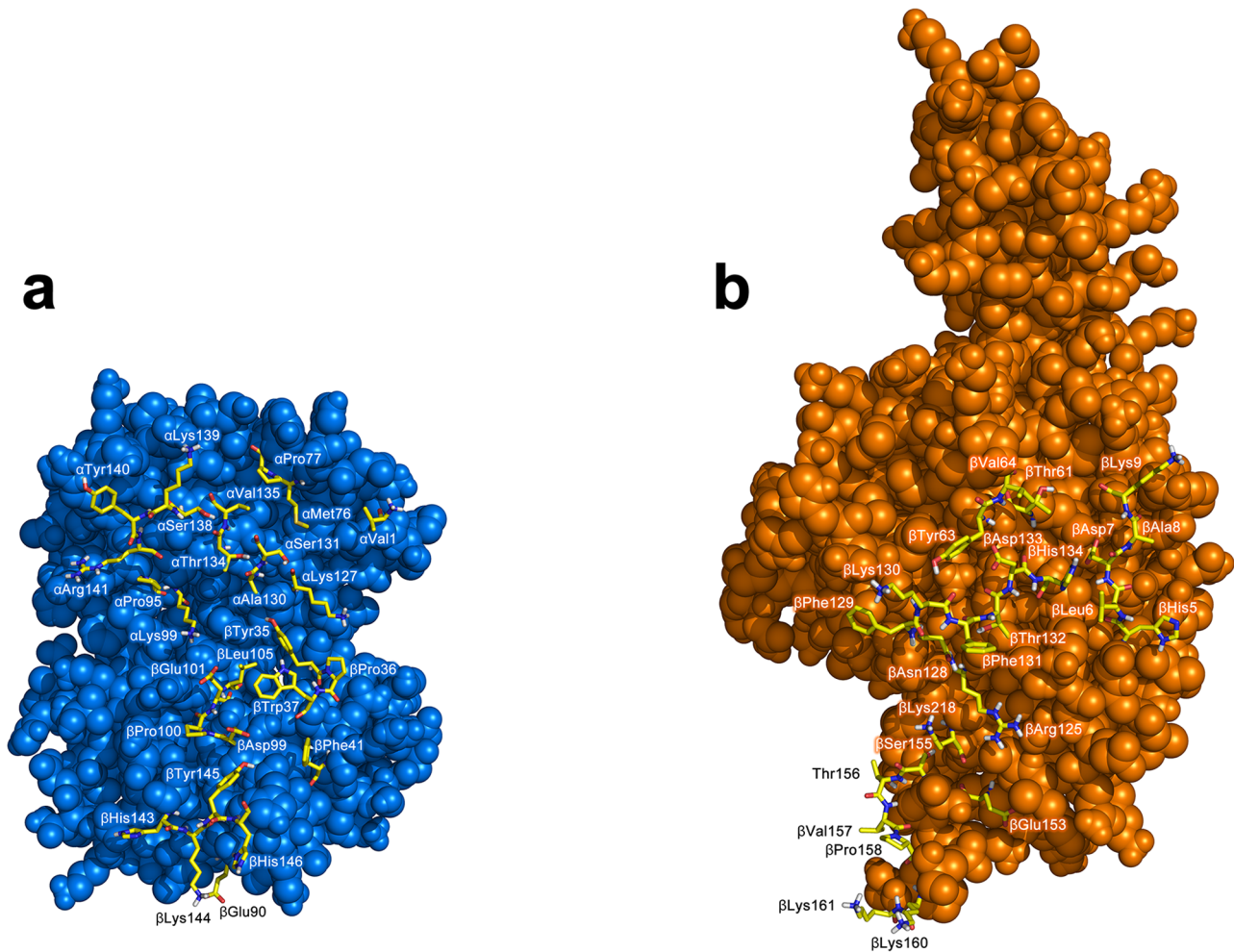


Figure 5. Residues at the binding interfaces of Hb and Hp from docking complexes of Hb-Hp are displayed as yellow colored sticks.
doi:10.1371/journal.pone.0062996.g005

residues. This result corroborates the fact that an equal share of residues had neutral and high polarity at the binding interface.

As for the Hb-Hp β complex there was an average of 35.6 ± 3.4 (ranging from 29 to 40) and 37.9 ± 4.6 (ranging from 31 to 45) residues of Hb and Hp β , respectively. The interface area occupied $1353.3 \pm 195.2 \text{ \AA}^2$ (ranging from 1079.4 to 1668.8) or roughly 8.1 and 9.6% of the SASA of Hb and Hp with SASA of 16716.4 ± 190.7 and $14157.2 \pm 224.5 \text{ \AA}^2$, respectively. The number of continuous interface residue segment for Hb-Hp β was 13.2 ± 1.9 (ranging from 10 to 15). The gap volume index of $3.8 \pm 0.6 \text{ \AA}$ for Hb-Hp β is lower than that of Hb-Hp, which is indicative of closer packing than that of the latter. The planarity of Hb-Hp β is roughly similar to that of Hb-Hp with a value of $3.6 \pm 0.4 \text{ \AA}$, also suggesting that the binding interface is not flat and may protrude into the respective binding partner. Similar to that of Hb-Hp, the results also suggested that the secondary structures at the binding interface of Hb-Hp β comprised of coils and α -helices. Furthermore, the relative distribution of the polarity of surface exposed residue revealed that before complexation there were 31, 67 and 92 residues belonging to the low, neutral and high polarity classes, respectively, or approximately 16.3%, 35.3% and 48.4%, respectively, of the total residues. After Hb-Hp β complex formation the buried residues or those situated at the binding interface are composed of 6, 8 and 4 residues, respectively, corresponding to

27.3%, 36.4% and 18.2%, respectively, of the residues. This result indicated that the absence of the α -chain led to structural perturbation of the β -chain that influenced the binding interface by shifting the polarity of interface residues towards lower polarity.

Identification of hot spot residues

Alanine scanning mutagenesis of protein-protein interfaces had indicated that the binding energy is not evenly distributed throughout the binding interface. It was found that there exist hot spots where certain residues exert major contributions to the binding energy of Hb-Hp complex [49,50]. Particularly, Thorn and Bogan [51,52] observed from their exhaustive collection of hot spots from alanine scanning mutagenesis data that hot spots are typically surrounded by residues with less energetic contribution to binding energy. The topology of such observation had the hotspot residue situated on the inside while its surrounding residues form the so-called O-ring. Such analysis revealed that hot spots are typically comprised of Trp, Tyr and Arg. These residues were found to be surrounded by aromatic rings whose plausible role is in the occlusion of bulk solvent [52].

In order to identify hot spots, the top ten complexes of both Hb-Hp and Hp β -Hp were subjected to computational alanine scanning mutagenesis using the FoldX plugin in Yasara in order to identify putative hot spot residues using $\Delta\Delta G_{\text{binding}} \geq 1.5 \text{ kcal/mol}$ as cut-off

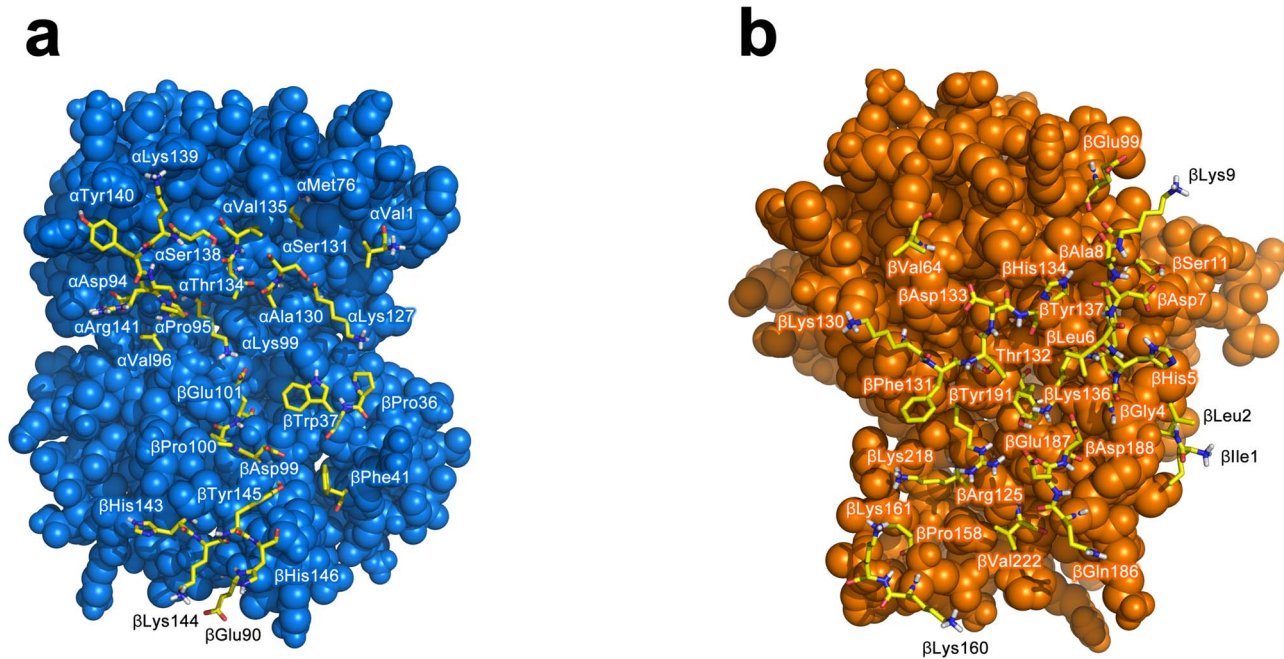


Figure 6. Residues at the binding interfaces of Hb and Hp $_{\beta}$ from docking complexes of Hb-Hp $_{\beta}$ are displayed as yellow colored sticks.

doi:10.1371/journal.pone.0062996.g006

criteria. The results strongly suggest that β Trp37 ($\Delta\Delta G_{\text{binding}} = 3.97, 2.74, 2.54, 2.25, 2.02$ and 1.61 kcal/mol) and β Tyr145 ($\Delta\Delta G_{\text{binding}} = 1.61$ and 2.5 kcal/mol) are hot spots of Hb while β Phe131 ($\Delta\Delta G_{\text{binding}} = 2.92, 2.7, 2.58, 2.54, 1.91, 1.89, 1.86$ and 1.71 kcal/mol) is a hot spot of Hp as judged from a frequency of at least 2 and at most 8 models (from the top ten complex for both Hb-Hp and Hp $_{\beta}$ -Hp) having $\Delta\Delta G_{\text{binding}} \geq 1.5$ for both Hb-Hp and Hp $_{\beta}$ -Hp complexes.

On the basis of molecular modeling analysis on the top ranked complex of Hb-Hp, it is observed that β Trp37 of Hb participates in π - π ring stacking interaction with two neighboring phenylalanines of Hp, β Phe129 and β Phe131, as well as engaging in a possible π -cation interaction with a nearby lysine of Hp, β Lys130 (Figure 7a). It is also interesting to note that both β Trp37 and β Phe131 are hot spots of each respective protein and both are interacting with one another suggesting the importance of this interacting region.

It is observed from Figure 7b that β Phe131 of Hp takes part in intermolecular π - π stacking interactions with aromatic residues of Hb, β Tyr35 and β Trp37, where the distance is 4 and 3.8 Å apart. Aside from this inner sphere of aromatic residues there also exists a second outer sphere of aromatic residues comprising of two phenylalanines, β Phe41 and β Phe42, where the former is approximately 5.9 Å from β Trp37 and the latter is 9 Å from the former. It is also interesting to note that when taking protein dynamics into consideration that the peripheral phenylalanine may possibly come into closer contact with β Tyr35 to form a more compact cluster of aromatic π - π stacking interactions.

The importance of π -cation interaction on protein stability [53,54] and function [55,56] is widely known. Burley and Petsko [57] analyzed the geometrical distances of amino groups (Lys, Arg, Asn, Gln and His) of side chains from nearby aromatic (Trp, Tyr and Phe) residues from the crystal structures of 33 proteins and their findings illuminated that favorable interaction occurs when the amino groups and aromatic residues are in the range of 3.4

and 6 Å apart. In our investigation, the distance between the side chains of β Trp37 and β Lys130 was measured in PyMol to be approximately 6 Å apart, thus corroborating a possible π -cation interaction. If protein dynamics is also taken into consideration such distances may change to allow both interacting partners to be in closer proximity.

Redox inactivation of Hb by Hp

The redox activity of Hb and its implications on hematological disorders are well known. Briefly, the reaction between Hb and hydrogen peroxide is known to form two intermediate products: (i) the ferryl heme iron, Fe(IV)=O and (ii) the Hb free radical, $\text{Hb}(\text{Fe}(\text{IV})=\text{O})$. Such reactive species are involved in oxidative stress-related human diseases. The residues governing such deleterious effects are often tyrosine residues, which have been referred to as redox cofactors in human hemoglobin [58].

To provide a structural account on the mechanistic details of these tyrosine residues at the binding interface, a detailed molecular modeling analysis was performed. The molecular models of Hb-Hp complex as obtained from protein-protein docking calculations revealed that the penultimate tyrosine residues, β Tyr145 (Figure 8a) and α Tyr140 (Figure 8b), are situated right at the binding interface. Such involvement of the penultimate tyrosine implicates the possibility of electron transfer from these tyrosine residues of Hb to accepting residues of Hp. Furthermore, it was observed that α Tyr42 of Hb (Figure 8b) as well as the heme prosthetic group of both the α and β -chains are located at a short distance from the Hb-Hp binding interface.

Implication of Hp α -chain in Hb-Hp interaction

In absence of the Hp α -chain, it was observed that there was some structural perturbation that led to slightly altered protein-protein interaction. For example, the π - π interactions of β Trp37 with the two phenylalanines (β Phe129 and β Phe131) of Hp were lost while forming a new π - π interaction with β His134. It is also

Table 2. List of residues at the binding interface of Hb-Hp complex.*

Residue	Frequency	Residue	Frequency
<i>Hemoglobin α</i>		<i>Haptoglobin β</i>	
Val1	8	His5	9
Met76	9	Leu6	10
Pro77	7	Asp7	9
Pro95	10	Ala8	10
Lys99	7	Lys9	9
Lys127	10	Thr61	9
Ala130	8	Tyr63	9
Ser131	9	Val64	10
Thr134	10	Arg125	9
Val135	10	Asn128	9
Ser138	10	Phe129	10
Lys139	10	Lys130	10
Tyr140	10	Phe131	10
Arg141	10	Thr132	9
		Asp133	9
<i>Hemoglobin β</i>		His134	10
Tyr35	10	Glu153	8
Pro36	9	Ser155	8
Trp37	10	Thr156	10
Phe41	7	Val157	10
Glu90	9	Pro158	10
Asp99	7	Lys160	10
Pro100	7	Lys161	8
Glu101	10	Lys218	10
Leu105	9		
His143	9		
Lys144	10		
Tyr145	10		
His146	10		

*Residues in bold text are those also found in the Hb-Hp β complex.
doi:10.1371/journal.pone.0062996.t002

interesting to note the presence of a nearby lysine (β Lys136) that may potentially form π -cation interaction with the indole ring of β Trp37 as well as the presence of a distant tyrosine (β Tyr137) of Hp. Nevertheless, the new interaction appears to be weaker than the former complex where the two aromatic rings of phenylalanines provided stronger stabilization. However, the removal of the α -chain brought forward a cluster of aromatic residues of Hp β -chain (β Phe12, β Tyr119, β His201 and β Trp208) onto the binding interface. Looking at α Tyr42, its distance from α Asp94 increased slightly but accessible to engage in redox transfer. Thus, the loss of the Hp α -chain led to perturbation of π - π interactions of β Trp37 with β Phe129 and β Phe131. As β Phe131 has been shown to be a hot spot residue, such perturbation is thus detrimental towards the Hb-Hp complex formation. This suggests the role of the Hp α -chain in maintaining the internal structural integrity of the Hp structure where its removal led to structural rearrangement of the structure, which affected the binding with Hb.

Table 3. List of residues at the binding interface of Hb-Hp β complex. *

Residue	Frequency	Residue	Frequency
<i>Hemoglobin α</i>		<i>Haptoglobin β</i>	
Val1	8	Ile1	8
Met76	8	Leu2	10
Asp94	7	Gly4	7
Pro95	10	His5	10
Val96	7	Leu6	10
Lys99	10	Asp7	10
Lys127	8	Ala8	10
Ala130	9	Lys9	10
Ser131	10	Ser11	9
Thr134	10	Val64	7
Val135	8	Glu99	8
Ser138	10	Arg125	10
Lys139	9	Lys130	10
Tyr140	8	Phe131	10
Arg141	10	Thr132	10
		Asp133	10
<i>Hemoglobin β</i>		His134	10
Pro36	8	Lys136	10
Trp37	10	Tyr137	9
Arg40	10	Pro158	8
Phe41	10	Lys160	10
Asp94	8	Lys161	7
His97	10	Gln186	10
Asp99	10	Glu187	10
Pro100	10	Asp188	7
Glu101	10	Tyr191	10
Asn139	10	Lys218	8
Ala142	9	Val222	8
His143	10		
Lys144	10		
Tyr145	10		
His146	10		

*Residues in bold text are those also found in the Hb-Hp complex.
doi:10.1371/journal.pone.0062996.t003

Comparison of modeled and crystal structure of Hb-Hp interaction

At the time of manuscript submission, the crystal structure of Hb-Hp complex was not yet available even though initial efforts attempted by Przybylska et al. [17] failed to obtain crystals that could diffract well enough for data collection. In absence of the crystal structure our study therefore represented a lucrative approach for shedding light on such important interaction. Nevertheless, the recently released crystal structure of porcine Hb-Hp complex (accession number 4F4O) by Andersen et al. [59] could thus be used as an external validation of the computational methodology described in our manuscript reminiscing that of the Critical Assessment of Predicted Interactions (CAPRI) [60], a community-wide assessment of computational methods for protein-protein docking in predicting protein-protein interactions for which its X-ray crystallographic structure has not yet been solved.

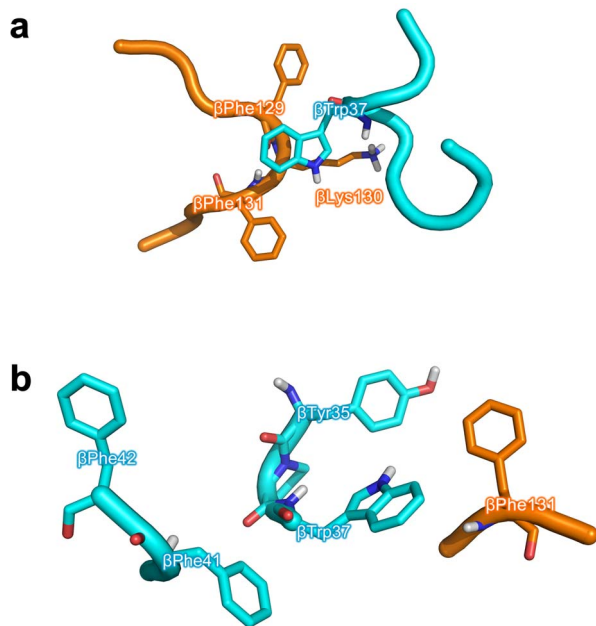


Figure 7. Molecular modeling analysis at the binding interface of the top ranked complex of Hb-Hp with particular focus on β Trp37 of Hb (a) and β Phe131 of Hp (b). The former panel shows β Trp37 of Hb participating in π - π ring stacking interaction with two neighboring phenylalanines of Hp, β Phe129 and β Phe131, as well as engaging in π -cation interaction with a nearby lysine of Hp, β Lys130. The latter panel shows β Phe131 of Hp taking part in intermolecular π - π stacking interactions with aromatic residues of Hb, β Tyr35 and β Trp37. In addition to the inner sphere of aromatic residues of Hb (comprising of β Tyr35 and β Trp37), a second outer sphere of aromatic residues of Hb (comprising of β Phe41 and β Phe42) is also present. doi:10.1371/journal.pone.0062996.g007

A comparative analysis of the modeled and crystal structure of Hb-Hp complex was performed by sequentially superimposing the crystal structure (chains A, B and C) with each of the top 10 modeled structures from HADDOCK protein-protein docking simulations. Results from superimposition of the structures indicated that models 1 through 10 had RMSD values of 10.6, 12.2, 11, 12.3, 12.5, 12.8, 12.8, 11.1, 10.9 and 12.2 Å, respectively, which had been aligned over 444, 437, 431, 433, 432, 426, 431, 443, 443 and 445 residues, respectively. It can be seen that the selected best Hb-Hp docking model or model 1 also possessed the lowest structural variation with respect to the crystal structure. Furthermore, the structure superimposition of model 1 with that of the crystal structure (Figure 9a) further corroborates the robustness of the methodology employed herein in predicting Hb-Hp interaction. It is worthy to note that the 10 top modeled structures were from the same cluster of 87 Hb-Hp docking structures with positional RMSD of 2.35 Å, which also suggests that the remaining 9 models also display similar overall binding topology as that observed from model 1.

It is observed that the modeled structure overlays nicely with the crystal structure where the Hp α -chain is positioned away from the Hb-Hp interface. Although the overall structure of both complexes provided good superimposition, the Hp α -chain did not overlay so well, which can be attributed to the truncated α -chain (13 residues missing) of the modeled structure in comparison to the crystal structure. This is in concomitant with the lack of a disulfide bridge formation between Cys15 of the Hp α -chain with that of its partner α -chain, which is not present in the model owing to the simplification made to the modeling performed herein. This may

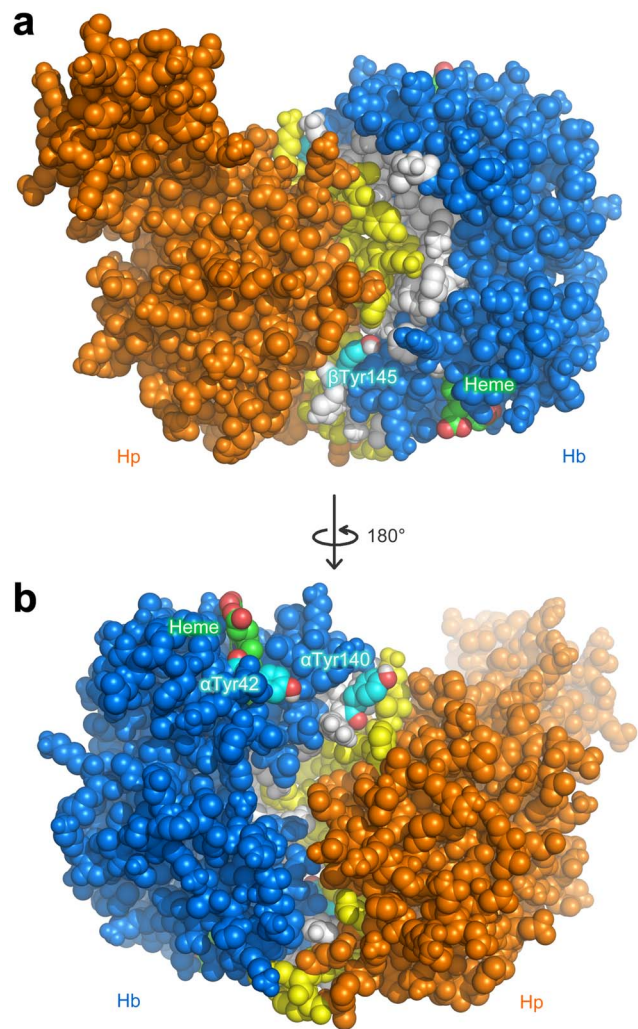


Figure 8. Molecular models of Hb-Hp complex as obtained from protein-protein docking calculations revealed that the penultimate tyrosine residues, β Tyr145 (a) and α Tyr140 (b), are situated right at the binding interface and are located on opposite side of the protein. α Tyr42 of Hb (b) as well as the heme prosthetic group of both α and β -chains are located at a distance from the binding interface. doi:10.1371/journal.pone.0062996.g008

partly account for the observed greater mobility in the Hp α -chain that was detrimental towards the structure superimposition of the modeled and crystal structures. Results from structure superimposition of the Hp structure alone from the modeled and crystal structures corroborate this point, as the structural variation of Hp modeled and crystal structure (Figure 9b) was relatively high with a calculated RMSD value of 9.29 Å while the structural variation of Hb modeled and crystal structure (Figure 9c) was significantly lower with an RMSD of 3.74 Å. Nevertheless, the main features of Hb-Hp interaction as elucidated from X-ray crystallography where the (1) Hb dimer contact area in Hb tetramers overlaps with those of the Hp-binding interface of Hb as well as (2) masking of redox residues of Hb upon Hp binding were provided by the modeled structures. In regards to the latter, the two penultimate tyrosines (i.e. β Tyr145 and α Tyr140), which was previously mentioned to be situated at the Hb-Hp binding interface of the modeled structure were indeed present in the crystal structure where Hp were found to mask those redox residues. Likewise,

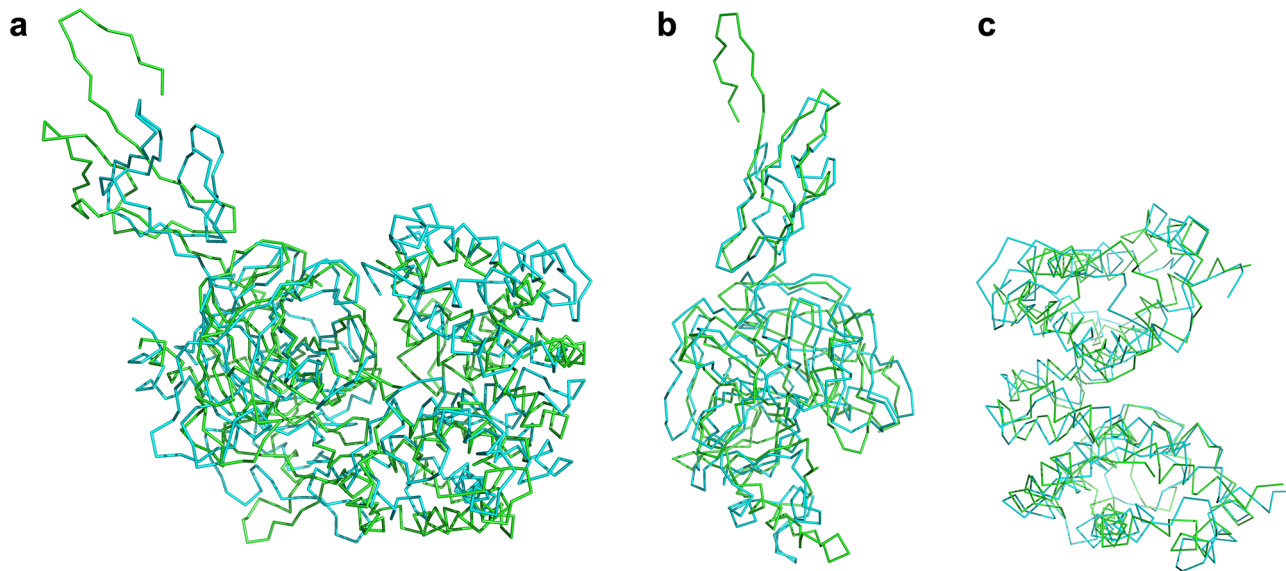


Figure 9. Structure superimposition of modeled (cyan) and crystal (green) structure of Hb-Hp complex (a) as well as Hp (b) and Hb (c) structures.

doi:10.1371/journal.pone.0062996.g009

α Tyr42, which was previously mentioned to be at a short distance from the binding interface were also present in the crystal structure at a similar distance away from the binding interface.

In comparison to the crystal structure of the porcine Hb-Hp complex, residues β Phe129, β Lys130 and β Phe131 of Hp from the human Hb-Hp complex (Figure 7a) was found to be different from the porcine complex where the former two residues were Leu and Asn instead of Phe and Lys of the human complex. In regards to β Trp37 as found in the human complex, Trp was also found at a comparable position of Hp from the porcine complex. All amino acid residues present at the aromatic cluster as shown in Figure 7b were found to be the same in both human and porcine complex. It should be noted that in the crystal structure of the porcine complex, the Phe residue from Hp of the porcine complex (i.e. corresponding to that of β Phe131 from Hp of the human complex) swings away from the aromatic clusters from Hb of the porcine complex when compared to Hb from the human complex. However, protein dynamics may allow the Phe residue from Hp of the porcine complex to swing out from the protein cavity and engage in interaction with the aromatic cluster.

Conclusions

Hb unleashes its reactivity and toxicity upon hemolysis. Hp counteracts the deleterious effects of Hb by binding and relaying Hb for clearance via CD163-mediated endocytosis by macrophages. The interaction of Hb and Hp represents one of the strongest interactions known in nature and the structural details of

such binding have yet to be fully elucidated. With the great advancements in molecular modeling it is possible to shed light on this important interaction through the use of several computational approaches. The initial structures of Hb and Hp was subjected to a steepest descent energy minimization their energetically favorable conformation was obtained by means of a preliminary steepest descent energy minimization and MD simulation. Finally, an ensemble of structures from the final 10 ns of MD simulation was cross-docked to yield a subsequent set of possible Hb-Hp complex. Post-analysis of these top ten complex provided pertinent information on the binding interface of Hb-Hp and Hb-Hp β , particularly that their interaction surface is not flat and protrudes well into each binding partner. Furthermore, it was also observed that the secondary structure at the interface takes the form of coils and α -helices. The results obtained herein are consistent with previously reported data on Hb and Hp binding. The robustness of the computational methodology described herein is further corroborated by the good superimposition of the modeled and crystal structures of Hb-Hp complexes. Such information provided structural insights on the binding modalities of Hb-Hp, which may be useful in the design of Hp mimics as Hb scavengers.

Author Contributions

Conceived and designed the experiments: CN LB. Performed the experiments: CN. Analyzed the data: CN LB. Contributed reagents/materials/analysis tools: VP. Wrote the paper: CN LB.

References

1. Vinogradov SN, Moens L (2008) Diversity of globin function: enzymatic, transport, storage, and sensing. *J Biol Chem* 283: 8773–8777.
2. Reeder BJ (2010) The redox activity of hemoglobins: from physiologic functions to pathologic mechanisms. *Antioxid Redox Signal* 13: 1087–1123.
3. Olsson MG, Allhorn M, Bulow L, Hansson SR, Ley D, et al. (2012) Pathological conditions involving extracellular hemoglobin: molecular mechanisms, clinical significance, and novel therapeutic opportunities for alpha(1)-microglobulin. *Antioxid Redox Signal* 17: 813–846.
4. Rother RP, Bell L, Hillmen P, Gladwin MT (2005) The clinical sequelae of intravascular hemolysis and extracellular plasma hemoglobin: a novel mechanism of human disease. *J Am Med Assoc* 293: 1653–1662.
5. Polonovski M, Jayle MF (1938) Existence dans le plasma sanguin d'une substance activant l'action peroxydasique de l'hémoglobine. *C R Acad Sc (Paris)* 129: 457.
6. Wicher KB, Fries E (2006) Haptoglobin, a hemoglobin-binding plasma protein, is present in bony fish and mammals but not in frog and chicken. *Proc Natl Acad Sci U S A* 103: 4168–4173.
7. Alayash AI (2011) Haptoglobin: Old protein with new functions. *Clin Chim Acta* 412: 493–498.
8. McCormick DJ, Atassi MZ (1990) Hemoglobin binding with haptoglobin: delineation of the haptoglobin binding site on the alpha-chain of human hemoglobin. *J Protein Chem* 9: 735–742.

9. Kazim AL, Atassi MZ (1981) Haemoglobin binding with haptoglobin. Localization of the haptoglobin-binding site on the alpha-chain of human haemoglobin. *Biochem J* 197: 507–510.
10. Hwang PK, Greer J (1979) Identification of residues involved in the binding of hemoglobin alpha chains to haptoglobin. *J Biol Chem* 254: 2265–2270.
11. Yoshioka N, Atassi MZ (1986) Haemoglobin binding with haptoglobin. Localization of the haptoglobin-binding sites on the beta-chain of human haemoglobin by synthetic overlapping peptides encompassing the entire chain. *Biochem J* 234: 453–456.
12. Lustbader JW, Arcoletto JP, Birken S, Greer J (1983) Hemoglobin-binding site on haptoglobin probed by selective proteolysis. *J Biol Chem* 258: 1227–1234.
13. Urushibara N, Kumazaki T, Ishii S (1992) Hemoglobin-binding site on human haptoglobin. Identification of lysyl residues participating in the binding. *J Biol Chem* 267: 13413–13417.
14. Chiao MT, Bezkorovainy A (1972) Interaction of modified haptoglobin with hemoglobin. *Biochim Biophys Acta* 263: 60–69.
15. Melamed-Frank M, Lache O, Enav BI, Szafrank T, Levy NS, et al. (2001) Structure-function analysis of the antioxidant properties of haptoglobin. *Blood* 98: 3693–3698.
16. Wejman JC, Hovsepian D, Wall JS, Hainfeld JF, Greer J (1984) Structure of haptoglobin and the haptoglobin-hemoglobin complex by electron microscopy. *J Mol Biol* 174: 319–341.
17. Przybylska M, Sheppard HM, Szilagyi S (1999) Crystallization of the haptoglobin-hemoglobin complex. *Acta Crystallogr D Biol Crystallogr* 55: 883–884.
18. Saxena A, Wong D, Diraviyam K, Sept D (2009) The basic concepts of molecular modeling. *Methods Enzymol* 467: 307–334.
19. Sansom C (1998) Extending the boundaries of molecular modeling. *Nat Biotechnol* 16: 917–918.
20. Isarankura-Na-Ayudhya C, Nantasenam C, Tantimongkolwat T, Worachartcheewan A, Yainoy S, et al. (2009) Roles of cysteine residue on chimeric green fluorescent protein: Implications on protein solubilization and fluorescent property. *Eur J Sci Res* 26: 577–593.
21. Suvannang N, Nantasenam C, Isarankura-Na-Ayudhya C, Prachayasittikul V (2011) Molecular docking of aromatase inhibitors. *Molecules* 16: 3597–3617.
22. Wu T, Wang XS, Cohen B, Ge H (2010) Molecular modeling of normal and sickle hemoglobins. *Int J Multiscale Comput Eng* 8: 237–244.
23. Pieraccini S, De Gonda R, Sironi M (2011) Molecular modeling of the inhibition of protein-protein interactions with small molecules: The IL2-IL2R α case. *Chem Phys Lett* 517: 217–222.
24. Yadavalli V, Mallela C, Subramanyam R (2011) Protein-protein interactions by molecular modeling and biochemical characterization of PSI-LHCl super-complexes from *Chlamydomonas reinhardtii*. *Mol Biosyst* 7: 3143–3151.
25. Lauria A, Tutone M, Ippolito M, Pantano L, Almerico AM (2010) Molecular modeling approaches in the discovery of new drugs for anti-cancer therapy: the investigation of p53-MDM2 interaction and its inhibition by small molecules. *Curr Med Chem* 17: 3142–3154.
26. Mishra S (2012) Computational prediction of protein-protein complexes. *BMC Res Notes* 5: 495.
27. Wass MN, Fuentes G, Pons C, Pazos F, Valencia A (2011) Towards the prediction of protein interaction partners using physical docking. *Mol Syst Biol* 7: 469.
28. Cooper CE, Schaer DJ, Buchler PW, Wilson MT, Reeder BJ, et al. (2012) Haptoglobin Binding Stabilizes Hemoglobin Ferryl Iron and the Globin Radical on Tyrosine β 145. *Antioxid Redox Signal*: In Press, doi:10.1089/ars.2012.4547.
29. Park SY, Yokoyama T, Shibayama N, Shiro Y, Tame JR (2006) 1.25 Å resolution crystal structures of human haemoglobin in the oxy, deoxy and carbonmonoxy forms. *J Mol Biol* 360: 690–701.
30. Politicelli F, Bocedi A, Minervini G, Ascenzi P (2008) Human haptoglobin structure and function – a molecular modelling study. *FEBS J* 275: 5648–5656.
31. Delano W (2002) PyMOL Release 0.99. Palo Alto, CA: DeLano Scientific LLC.
32. Kovalevsky AY, Chatake T, Shibayama N, Park SY, Ishikawa T, et al. (2010) Direct determination of protonation states of histidine residues in a 2 Å neutron structure of deoxy-human normal adult hemoglobin and implications for the Bohr effect. *J Mol Biol* 398: 276–291.
33. Chatake T, Shibayama N, Park SY, Kurihara K, Tamada T, et al. (2007) Protonation states of buried histidine residues in human deoxyhemoglobin revealed by neutron crystallography. *J Am Chem Soc* 129: 14840–14841.
34. Dolinsky TJ, Nielsen JE, McCammon JA, Baker NA (2004) PDB2PQR: an automated pipeline for the setup of Poisson-Boltzmann electrostatics calculations. *Nucleic Acids Res* 32: W665–667.
35. Olsson MHM, Sondergaard CR, Rostkowski M, Jensen JH (2011) PROPKA3: Consistent Treatment of Internal and Surface Residues in Empirical pKa Predictions. *J Chem Theor Comput* 7: 525–537.
36. Christen M, Hunenberger PH, Bakowies D, Baron R, Burgi R, et al. (2005) The GROMOS software for biomolecular simulation: GROMOS05. *J Comput Chem* 26: 1719–1751.
37. Hess B, Kutzner C, van der Spoel D, Lindahl E (2008) GROMACS 4: Algorithms for Highly Efficient, Load-Balanced, and Scalable Molecular Simulation. *J Chem Theor Comput* 4: 435–447.
38. Berendsen HJC, Postma JPM, van Gunsteren WF, DiNola A, Haak JR (1984) Molecular dynamics with coupling to an external bath. *J Chem Phys* 81: 3684–3690.
39. Barker JA, Watts RO (1973) Monte Carlo studies of the dielectric properties of water-like models. *Mol Phys* 26: 789–792.
40. Hess B, Bekker H, Berendsen HJC, Fraaije JGEM (1997) LINCS: A linear constraint solver for molecular simulations. *J Comput Chem* 18: 1463–1472.
41. Dominguez C, Boelens R, Bonvin AM (2003) HADDOCK: a protein-protein docking approach based on biochemical or biophysical information. *J Am Chem Soc* 125: 1731–1737.
42. de Vries SJ, van Dijk M, Bonvin AM (2010) The HADDOCK web server for data-driven biomolecular docking. *Nat Protoc* 5: 883–897.
43. Krissinel E, Henrick K (2005) PISA (Protein interfaces, surfaces and assemblies) website. Available: http://www.ebi.ac.uk/pdbe/prot_int/pistart.html. Accessed 2012 Jan 15.
44. Reynolds C, Damerell D, Jones S (2009) ProtorP: a protein-protein interaction analysis server. *Bioinformatics* 25: 413–414.
45. Van Durme J, Delgado J, Stricher F, Serrano L, Schymkowitz J, et al. (2011) A graphical interface for the FoldX forcefield. *Bioinformatics* 27: 1711–1712.
46. Guerois R, Nielsen JE, Serrano L (2002) Predicting changes in the stability of proteins and protein complexes: a study of more than 1000 mutations. *J Mol Biol* 320: 369–387.
47. Krieger E, Koraimann G, Vriend G (2002) Increasing the precision of comparative models with YASARA NOVA – a self-parameterizing force field. *Proteins* 47: 393–402.
48. Vacic V, Oldfield CJ, Mohan A, Radivojac P, Cortese MS, et al. (2007) Characterization of molecular recognition features, MoRFs, and their binding partners. *J Proteome Res* 6: 2351–2366.
49. Clackson T, Wells JA (1995) A hot spot of binding energy in a hormone-receptor interface. *Science* 267: 383–386.
50. DeLano WL (2002) Unraveling hot spots in binding interfaces: progress and challenges. *Curr Opin Struct Biol* 12: 14–20.
51. Thorn KS, Bogan AA (2001) ASEdb: a database of alanine mutations and their effects on the free energy of binding in protein interactions. *Bioinformatics* 17: 284–285.
52. Bogan AA, Thorn KS (1998) Anatomy of hot spots in protein interfaces. *J Mol Biol* 280: 1–9.
53. Gallivan JP, Dougherty DA (1999) Cation- π interactions in structural biology. *Proc Natl Acad Sci U S A* 96: 9459–9464.
54. Anbarasu A, Prasad VR, Sathpathy S, Sethumadhavan R (2009) Influence of cation- π interactions to the structural stability of prokaryotic and eukaryotic translation elongation factors. *Protoplasma* 238: 11–20.
55. Zacharias N, Dougherty DA (2002) Cation- π interactions in ligand recognition and catalysis. *Trends Pharmacol Sci* 23: 281–287.
56. Scrutton NS, Raine AR (1996) Cation- π bonding and amino-aromatic interactions in the biomolecular recognition of substituted ammonium ligands. *Biochem J* 319 (Pt 1): 1–8.
57. Burley SK, Petsko GA (1986) Amino-aromatic interactions in proteins. *FEBS Lett* 203: 139–143.
58. Reeder BJ, Grey M, Silaghi-Dumitrescu RL, Svistunenko DA, Bulow L, et al. (2008) Tyrosine residues as redox cofactors in human hemoglobin: implications for engineering nontoxic blood substitutes. *J Biol Chem* 283: 30780–30787.
59. Andersen CB, Torvund-Jensen M, Nielsen MJ, de Oliveira CL, Hershleth HP, et al. (2012) Structure of the haptoglobin-haemoglobin complex. *Nature* 489: 456–459.
60. Janin J, Henrick K, Moult J, Eyck LT, Sternberg MJ, et al. (2003) CAPRI: a Critical Assessment of PRedicted Interactions. *Proteins* 52: 2–9.